

Special Section on Drug Delivery Technologies

In Vivo Imaging of Small Molecular Weight Peptides for Targeted Renal Drug Delivery: A Study in Normal and Polycystic Kidney Diseased Mice

Stephen C. Lenhard,¹ Allen McAlexander,¹ Anthony Virtue,¹ William Fieles, Tina Skedzielewski, Mary Rambo, Han Trinh, Shih-Hsun Cheng, Hyundae Hong, Albert Isidro-Llobet, Alan Nadin, Robert Geske, Jean-Louis Klein, Dennis Lee, Beat M. Jucker, and Erding Hu

Bioimaging (S.C.L., T.S., M.R., S.-H.C., H.H., B.M.J.), Renal Discovery Group, Future Pipeline Discovery (A.V., E.H.), Experimental Cell and Tissue Biology, Target and Pathway Validation (W.F., H.T., R.G., J.-L.K.), Drug Delivery (A.M., D.L.), and Drug Design and Selection (A.I.-L., A.N.), GlaxoSmithKline plc, Collegeville, Pennsylvania

Received January 31, 2019; accepted March 18, 2019

ABSTRACT

Autosomal dominant polycystic kidney disease (ADPKD) is a leading monogenetic cause of end-stage renal disease with limited therapeutic repertoire. A targeted drug delivery strategy that directs a small molecule to renal niches around cysts could increase the safety margins of agents that slow the progression of ADPKD but are poorly tolerated due to extrarenal toxicity. Herein, we determined whether previously characterized lysine-based and glutamic acid-based megalin-binding peptides can achieve renal-specific localization in the juvenile cystic kidney (JCK) mouse model of polycystic kidney disease and whether the distribution is altered compared with control mice. We performed *in vivo* optical and magnetic resonance imaging studies using peptides conjugated to the VivoTag 680 dye and demonstrated that megalin-interacting peptides distributed almost exclusively to the kidney cortex in both normal and JCK

mice. Confocal analysis demonstrated that the peptide-dye conjugate distribution overlapped with megalin-positive renal proximal tubules. However, in the JCK mouse, the epithelium of renal cysts did not retain expression of the proximal tubule markers aquaporin 1 and megalin, and therefore these cysts did not retain peptide-dye conjugates. Furthermore, human kidney tumor tissues were evaluated by immunohistochemistry and revealed significant megalin expression in tissues from patients with renal cell carcinoma, raising the possibility that these tumors could be treated using this drug delivery strategy. Taken together, our data suggest that linking a small-molecule drug to these carrier peptides could represent a promising opportunity to develop a new platform for renal enrichment and targeting in the treatment of ADPKD and certain renal carcinomas.

Introduction

Autosomal dominant polycystic kidney disease (ADPKD) is the most common inherited cause of kidney disease, afflicting greater than 12 million people worldwide (Chapman et al., 2015). The development and uncontrolled growth of fluid-filled cysts within both kidneys leads to disorganization of

the highly structured organ. As a result, kidney function becomes compromised, leading to kidney failure in 50% of patients within the fifth decade of life. An attractive therapeutic approach for ADPKD is the repurposing of already approved antiproliferative agents typically used in cancer. In fact, a wide range of these agents has been shown to be efficacious in preclinical models of ADPKD (Muller and Benzing, 2018). However, these therapeutics have failed to demonstrate clinical benefits primarily due to poor tolerability and/or dose-limiting, mechanism-based extrarenal

¹S.L., A.M., and A.V. contributed equally to this work.
<https://doi.org/10.1124/jpet.119.257022>

ABBREVIATIONS: aa, amino acid; ADPKD, autosomal dominant polycystic kidney disease; AQP1, aquaporin-1; ccRCC, clear cell renal cell carcinoma; chrRCC, chromophobe renal cell carcinoma; DAPI, 4',6'-diamidino-2-phenylindole dihydrochloride; DICOM, digital imaging and communications in medicine; DIPEA, *N,N*-diisopropylethylamine; DMF, *N,N*-dimethylformamide; Fmoc, 9-fluorenylmethoxycarbonyl; FMT, fluorescence molecular tomography; FOV, field of view; HCTU, 2-(6-chloro-1-*H*-benzotriazole-1-yl)-1,1,3,3-tetramethylammonium hexafluorophosphate; IHC, immunohistochemistry; JCK, juvenile cystic kidney; MRI, magnetic resonance imaging; NIR, near infrared; pRCC, papillary renal cell carcinoma; RARE, rapid acquisition with relaxation enhancement; RCC, renal cell carcinoma; TE, echo time; TFA, trifluoroacetic acid; 3D, three-dimensional; TMA, tumor tissue microarray; TR, repetition time.

toxicity (Weimbs et al., 2018). The ability to selectively target the kidneys for drug delivery would minimize exposure in other tissues, thus enabling the development of novel and more efficacious drugs or the repurposing of preapproved antiproliferative therapeutics by reducing the extrarenal side effects associated with these agents.

One strategy to facilitate renal drug targeting is the conjugation of therapeutics to K-containing and E-containing peptides. Wischnjow et al. (2016) demonstrated that a short KE-containing peptide is capable of renal targeting in normal mice via megalin-mediated endocytosis. It is well established that small molecular weight peptides and low molecular weight proteins are reabsorbed from the filtrate via receptors on the apical surface of proximal tubule cells by the integral membrane protein megalin (Christensen and Birn, 2002). Megalin is a central driver of filtered peptide/protein reabsorption into the proximal tubule epithelium by facilitating their endocytosis via a series of downstream effector proteins (De et al., 2014). The importance of megalin in driving reabsorption of peptides from the filtrate is underscored by the albuminuria and low molecular weight proteinuria in megalin knockout mice (Lehste et al., 1999). Given the vital role of megalin in peptide reabsorption, megalin-binding peptides may serve as versatile scaffolds to enable selective renal targeting. Indeed, a series of K- and E-containing small peptides have been shown to selectively deliver small molecules to the renal cortex in rat and multiple mouse strains (Wischnjow et al., 2016). The genetic knockout of megalin reduced renal retention of these labeled peptides, confirming the role of megalin in the reabsorption of these peptides from the filtrate.

In the present study, we employed a novel imaging modality to evaluate the kidney distribution of two KE-containing small peptides in both control mice and a well-established model of ADPKD, juvenile cystic kidney (JCK) mice. An optical and MRI coregistration analysis was carried out to quantify the kidney signal distribution followed by high-resolution confocal imaging analysis to determine whether small peptide sequences can target a near-infrared (NIR) dye to specific regions/cells of the kidney where cysts typically form. Finally, we examined the possible utility of these peptides in other kidney diseases by assessing the presence of megalin within human kidney neoplasms such as renal cell carcinoma (RCC).

Materials and Methods

Synthesis of Targeting Peptides [Amino-hexanoic-(KKEEE)_n-Amide] and VivoTag 680 XL Dye Conjugation. VivoTag 680 XL (PerkinElmer, Waltham, MA) is a NIR dye ideally suited for in vivo imaging. However, the synthesis of N-terminal labeled peptides can be challenging due to the high cost of the VivoTag 680 XL carboxylic acid building block and the use of a large excess of reagent typical of solid-phase peptide synthesis. Instead, an inverse approach was applied in which 0.3–0.5 Eq VivoTag 680 dye was used, and the corresponding tagged and untagged peptides were easily separated by semipreparative high-performance liquid chromatography (PLC 2020 Purification System; Gilson, Middleton, WI).

Resin-bound untagged peptides were obtained by the 9-fluorenylmethoxycarbonyl (Fmoc)/^tBu solid-phase peptide synthesis strategy on a Novabiochem Rink Amide AM Polystyrene Resin (0.05 mmol, 0.69 mmol/g; EMD Biosciences, San Diego, CA) using the Liberty 1 Microwave Peptide Synthesizer (CEM Corporation, Matthews, NC). Each amino acid was coupled once using the following conditions: Fmoc-amino acid [2.5 ml, 10 Eq, 0.2 M in *N,N*-dimethylformamide (DMF); Millipore Sigma, Burlington, MA], 2-(6-chloro-1-*H*-benzotriazole-1-yl)-1,1,3,3-tetramethylammonium hexafluorophosphate (HCTU) (1.0 ml, 10 Eq, 0.5 M in DMF; Chem-Impex, Wood Dale, IL), *N,N*-diisopropylethylamine (DIPEA) (1 ml, 10 Eq, 1 M in *N*-methyl-2-pyrrolidone; Sigma-Aldrich, St. Louis, MO) at 75°C for 10 minutes. Fmoc group removals were performed using 20% piperidine in DMF. Fmoc-Amino-hexanoic acid was coupled manually using HATU (1-[Bis(dimethylamino)methylene]-1*H*-1,2,3-triazolo[4,5-*b*]pyridinium 3-oxid hexafluorophosphate, *N*-[(dimethylamino)-1*H*-1,2,3-triazolo-[4,5-*b*]pyridin-1-ylmethylene]-*N*-methylmethanaminium hexafluorophosphate *N*-oxide) as opposed to HCTU.

Aliquots of resin were then labeled with VivoTag 680 XL Fluorochrome (0.3–0.5 Eq) in DMF using PyBOP (benzotriazol-1-yl-oxytrypyrrolidinophosphonium hexafluorophosphate; Fluorchem, Derbyshire, UK), HOAt (1-hydroxy-7-azabenzotriazole; Fluorchem), and DIPEA as coupling reagents for 90 minutes at room temperature. Cleavage from the solid support and final deprotection was performed with TFA-H₂O (95:5) for 90 minutes at room temperature. The solvent was then removed under reduced pressure, and the resulting crude peptides were purified by semipreparative high-performance liquid chromatography (solvent A = 0.1% TFA in water; solvent B = 0.1%TFA/90% acetonitrile/10% water) and freeze dried. The desired labeled peptides were characterized by liquid chromatography-mass spectrometry (>90% purity):

GSK601A (KKEEE)₂K: 8.3 mg (41% yield)

GSK599A (KKEEE)₃K: 6.7 mg (54% yield).

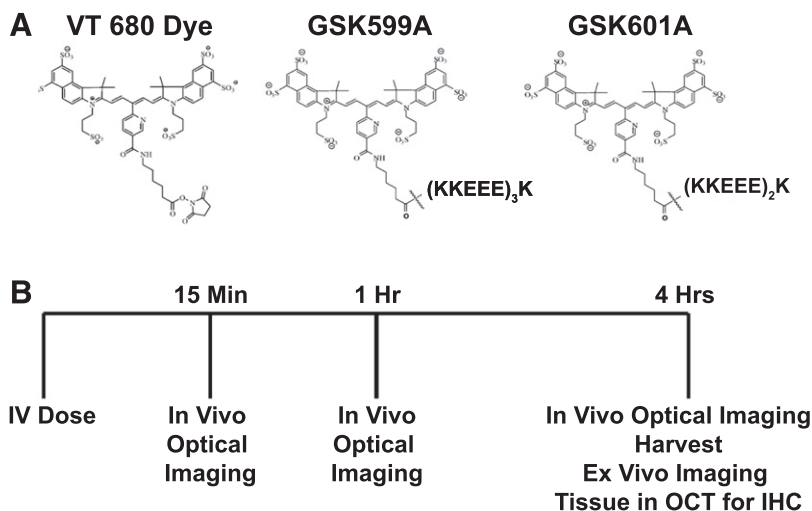


Fig. 1. Optical imaging study design and structures for VivoTag 680 dye, GSK599A, and GSK601A. (A) VivoTag 680 control dye, GSK601A (KKEEE)₂K, and GSK599A (KKEEE)₃K peptide-dye conjugate structures. (B) In vivo optical imaging study design denoting imaging timepoints after intravenous (IV) injection. Hr, hour; Hrs, hours.

In Vivo Optical Imaging. All mouse studies were approved by the GlaxoSmithKline Institutional Animal Care and Use Committee. Eight-week-old female SKH1 hairless mice (Charles River Laboratories, Horsham, PA) were used as control mice and 12-week-old male JCK mice (Crown BioScience, San Diego, CA) were used as disease model mice. Mice were anesthetized with 2% isoflurane and 1 l/min medical grade air for in vivo imaging. Mice were injected via tail vein with the control dye, VivoTag 680, GSK601A, or GSK599A (Fig. 1A). Each mouse received 200 μ g of peptide-dye conjugate, which was injected into the tail vein in 100 μ l of PBS. In vivo optical imaging (IVIS Spectrum-CT; PerkinElmer) was performed at 15 minutes, 1 hour, and 4 hours postinjection (Fig. 1B). After 4-hour postdose in vivo optical imaging, mice were euthanized, and brain, heart, liver, spleen, and kidneys were excised for ex vivo optical imaging in the IVIS Spectrum-CT and Odyssey Imaging Systems (LI-COR, Lincoln, NE). Upon completion of ex vivo imaging, the organs were placed in optimal cutting temperature compound (OCT) and frozen at -80°C for preservation for confocal imaging and analysis.

In Vivo/Ex Vivo Imaging. In vivo and ex vivo optical imaging were performed using a two-dimensional IVIS-Spectrum-CT system. After a white light photographic image was acquired, a fluorescent image was acquired using the following parameters: excitation filter, 675 nm; emission filter, 720 nm; f-stop, 2; exposure time, 3 seconds; and field of view (FOV), 13.4 cm. In vivo and ex vivo image analysis was performed using Living Image Software (version 4.5.2; PerkinElmer). For purposes of coregistering MRI with optical imaging, in vivo optical imaging was performed using a fluorescence molecular tomography (FMT) system (PerkinElmer). After the animal preparation, the mice were transferred to the holding platform of the optical scanner, and anesthesia was maintained with 0.5%–2% isoflurane using an appropriate gas carrier nose cone installed in the scanner. Fluorescence images were acquired using the following image acquisition parameters.

FMT excitation/emission wavelengths were 670/688 nm, the maximum power of the class 3b laser was 80 mW, and cassette depth was 15 mm, and there were \sim 100–120 excitation points in the scanfield. The collected fluorescence data were reconstructed using TrueQuant version 3.0 software (PerkinElmer) for the quantification of the three-dimensional (3D) fluorescence signal within an area/region of interest.

High-resolution ex vivo optical imaging of kidneys was also performed using the Li-Cor Odyssey Imager with an initial low-resolution (337 μ m) scout image on the lowest quality scan setting (\sim 1- to 1.5-minute acquisition time) for the purpose of properly locating the kidneys in the scan field prior to acquiring the high-resolution scan. The high-resolution (21 μ m) scan was acquired using the highest quality scan setting with a total acquisition time of approximately 8–10 minutes. Image Studio software version 5.2 was used for image acquisition.

MRI was performed on a 9.4-tesla horizontal bore system (Bruker Biospin, Billerica, MA). Prior to the start of the imaging session, mice were physiologically monitored in the FMT cassette with ECG leads. A gradient echo tripilot sequence was used to generate scout imaging. A two-dimensional RARE (rapid acquisition with relaxation enhancement) sequence [repetition time (TR), 1758 milliseconds; echo time (TE), 56 milliseconds; FOV, 78.85 \times 78.85 mm; image matrix, 256 \times 256] was followed with a 3D TurboRARE sequence (TR, 200 milliseconds; TE, 27 milliseconds; FOV, 78.85 \times 19.71 \times 78.85 mm; image matrix, 256 \times 64 \times 256) and a 3D FLASH sequence (fast low-angle shot) (TR, 16.1 milliseconds; TE, 5.4 milliseconds; FOV, 78.85 \times 19.71 \times 78.85 mm; image matrix, 256 \times 64 \times 256) to generate 3D images of the mice.

Coregistration of FMT/Magnetic Resonance Images. The spatial coregistration of the MRI and FMT images used a single software platform, VivoQuant (version 2.5; Invivo, Boston, MA). VivoQuant is capable of handling multiple DICOM (digital imaging and communications in medicine) image inputs from different modalities and allows users to adjust the relative spatial position for each image input. FMT images were exported to 16-bit DICOM format by the TrueQuant version 3.0 software (PerkinElmer). Multiple DICOM files and MRI raw data were imported into the VivoQuant data browser. The reorientation/registration tool was used to manually align multiple image datasets.

Confocal Microscopy. Blocks of tissue, previously frozen in liquid nitrogen and stored at -80°C , were placed in a cryostat and allowed to warm to a chamber temperature of -13°C . Six-micrometer sections were cut onto cold slides and warmed briefly to melt then were returned to the cryostat until all sections were cut. Once all sections were cut, the slides were removed from the cryostat, warmed until melted, and placed in a humidified chamber for fixation and antibody incubations. Sections were fixed in 4% paraformaldehyde for 15 minutes then washed in PBS for an additional 15 minutes. The slides were then blocked for 15 minutes in 1% bovine serum albumin. Slides were washed in PBS then incubated in the following mixture of primary antibodies diluted in 1% bovine serum albumin for 1 hour at room temperature: 1 μ g/ml rabbit anti-aquaporin 1 (AQP1) (catalog number Ab 2219; EMD Millipore) conjugated with Alexa Fluor 488 using the Invitrogen Zenon Labeling Kit (catalog number Z25302; Thermo Fisher Scientific, Waltham, MA), and 1 μ g/ml rabbit anti-megalin (catalog number 76969; Abcam, Cambridge, MA) labeled with Alexa Fluor 568 using the Zenon Kit (catalog number Z25306; Invitrogen). Slides were washed for 15 minutes in PBS then mounted and coverslipped using Invitrogen ProLong Gold with 4',6'-diamidino-2-phenylindole dihydrochloride (DAPI) (catalog number P36935; Thermo Fisher Scientific). Slides were viewed and imaged on a LSM 780 Confocal Microscope (Carl Zeiss Microscopy, Thornwood, NY).

Human Tissue Immunohistochemistry for Megalin Expression. Human tissues used in these studies were approved at GlaxoSmithKline plc. All donors provided written informed consent for use of their samples, and the collection and use of the samples received institutional review board (or ethics committee) approval. A human kidney tumor tissue microarray (TMA) (catalog number Z7020054; Biochain Institute, Inc., Hayward, CA) was used for these studies; each core of the array had a diameter of 1.5 mm, and the paraffin sections were 4 μ m thick. The TMA included neoplastic and non-neoplastic tissues (Table 1). Most diagnoses were represented by cores from multiple patients, and each patient's sample was provided in duplicate. All tumors were renal primaries, with no regional lymph node metastasis and no distant metastasis. Immunohistochemistry of the paraffin section TMA was performed on an automated staining platform (Discovery Ultra; Ventana Medical Systems, Tucson, AZ). Briefly, the staining protocol included deparaffinization, high pH antigen retrieval (Ultra CCI, catalog number 950-224; Ventana Medical Systems), protein block (SEA BLOCK blocking buffer, catalog number 37527; Thermo Fisher Scientific), incubation with either a rabbit anti-megalin antibody (catalog number A76969; Abcam) or nonimmune rabbit IgG (catalog number AB-105-C; R&D Systems, Minneapolis, MN) at 0.06 μ g/ml, detection with an alkaline phosphatase conjugated anti-rabbit IgG secondary antibody (UltraMap, catalog number 760-4314; Ventana Medical Systems), antigen visualization (Discovery Red, catalog number 760-228; Ventana Medical Systems), and hematoxylin nuclear counterstain (Hematoxylin II, catalog number 790-2208; Ventana Medical Systems). Slides were air dried and then coverslipped with a synthetic mounting media. A TMA slide was stained for morphologic assessment using H&E. Slides were scanned at 40 \times on a Nanozoomer (Hamamatsu, Hamamatsu, Japan); images (Fig. 6) were extracted from the scans.

Separate studies were performed to evaluate megalin and AQP1 coexpression in selected non-neoplastic and clear cell RCC (ccRCC) tumors. For these studies, non-neoplastic renal tissue from a 67-year-old female

TABLE 1
Megalin protein expression in human renal tumors

Diagnosis by IHC evaluation of megalin expression	Case Patients	Megalin-Positive	
		<i>n</i>	%
Noncancerous kidney biopsy	4	4	100
ccRCC	20	18	90
pRCC	7	4	57
Transitional cell carcinoma	3	0	0
chRCC	3	0	0

was obtained from the National Disease Research Interchange (we acknowledge the use of this tissue procured by the National Disease Research Interchange with support from National Institutes of Health grant U42-OD-11158). Additionally, ccRCC tissue from a 63-year-old male was received from the MT Group (Van Nuys, CA). In both case, patient samples were fixed in 10% neutral buffered formalin and processed to paraffin block using standard histologic technique; paraffin sections were made at 4 μm and collected on glass slides. Immunohistochemistry was carried out on the staining platform described above, but a multiplex fluorescent approach was used to demonstrate the expression and distribution of two separate proteins: megalin and AQP1. Briefly, the staining protocol included deparaffinization, high pH antigen retrieval (Ultra CCI, catalog number 950-224; Ventana Medical Systems), protein block (SEA BLOCK blocking buffer, catalog number 37527; Thermo Fisher Scientific), incubation with either a cocktail that included rabbit anti-megalin antibody (catalog number A76969; Abcam) and mouse anti-AQP1 (catalog number A9566; Abcam) or a cocktail of nonimmune rabbit IgG (catalog number AB-105-C; R&D Systems) and nonimmune mouse IgG2B (catalog number Ab18428; Abcam); all antibodies and isotype negative controls were used at 0.25 $\mu\text{g}/\text{ml}$. Secondary antibody detection was applied as a cocktail of goat anti-rabbit IgG conjugated to Alexa Fluor 594 (catalog number A-11037; Thermo Fisher Scientific) and goat anti-mouse IgG2B conjugated to Alexa Fluor 488 (catalog number A-21141; Thermo Fisher); both were applied at 6 $\mu\text{g}/\text{ml}$. Slides were mounted using ProLong Gold with DAPI (catalog number P36935; Thermo Fisher Scientific) and viewed under fluorescent light using a Leica DM6000-B Microscope (Leica Microsystems, Buffalo Grove, IL); images were captured using Leica LAS X Software (Leica Microsystems).

Statistical Analysis. All statistical analysis was performed using GraphPad Prism version 6.0 software (GraphPad, San Diego, CA).

Results

Distribution of Renal Targeting KE Peptide in Control Mice. Two KE peptides [11 and 16 amino acids (aa)] were conjugated to VivoTag 680 dye to enable in vivo NIR imaging and these peptide-dye conjugates were injected via an intravenous bolus (Fig. 1). In healthy control mice, optical imaging revealed that both GSK599A and GSK601A peptide-conjugated dyes preferentially localized to the kidney 4 hours postinjection (Fig. 2, A and B), while unconjugated VivoTag 680 was not detectable in the kidney at this time. Serial in vivo optical imaging revealed that an unconjugated VivoTag 680 dye renal signal was only observable 15 minutes post-injection in the kidney, but the signal was reduced to near-baseline levels by the 1-hour timepoint. In contrast, both GSK601A and GSK599A conjugates remained localized to the kidney at 15 minutes, 1 hour, and 4 hours postdose (Fig. 2B), while moderately faster renal clearance was observed in GSK601A-treated animals versus GSK599-treated animals.

Organs harvested for ex vivo optical imaging after the 4-hour postdose timepoint revealed that the unconjugated VivoTag 680 dye signal was present primarily in liver and kidney, but that very low levels were also detectable in brain, heart, and spleen (Fig. 2, C and D). In marked contrast, a strong signal was present predominantly in kidneys of GSK601A- and GSK599A-dosed animals, with far lower signal intensity present in liver, brain, heart, and spleen (Fig. 2, C and D). A modest, nonsignificant increase in optical signal was observed in the GSK601A group compared with the GSK599A group (Fig. 2D). Divergent from the in vivo optical imaging (Fig. 2B), a slightly more intense signal was observed for

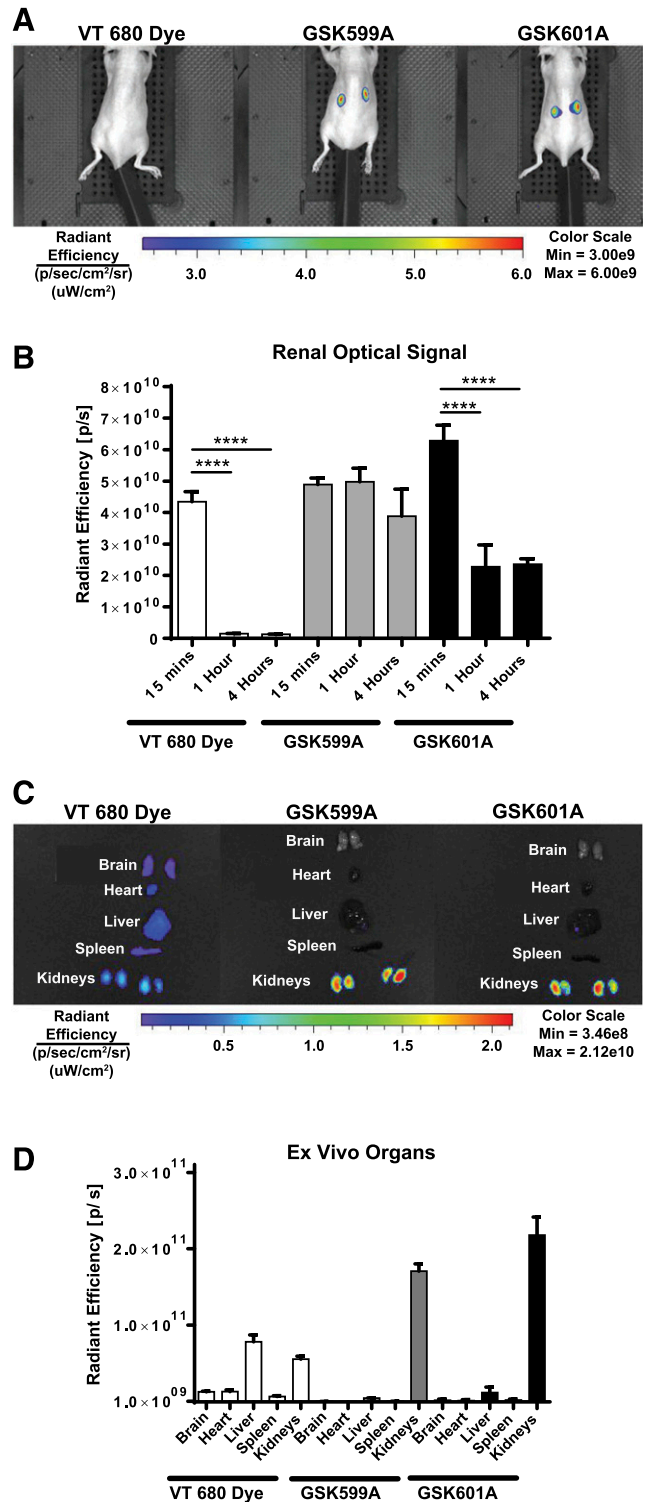


Fig. 2. In vivo and ex vivo optical imaging in control mice. (A) Representative VivoTag 680 dye, GSK599A, and GSK601A in vivo optical images 4 hours postinjection. (B) Renal optical signal at 15 minutes, 1 hour, and 4 hours postinjection. $n = 4-6$; error bars indicate mean \pm S.E.M. **** $P < 0.0001$ (one-way ANOVA with a multiple comparison test). (C) Representative ex vivo images of brain, heart, liver, spleen, and kidneys in mice treated with VivoTag 680 dye, GSK599A, and GSK601A. (D) Ex vivo organ optical signals in groups treated with VivoTag 680 dye vs. those treated with GSK599A and GSK601. Max, maximum; Min, minimum.

GSK601A compared with GSK599A with ex vivo imaging (Fig. 2D). This may reflect the difference in optimal measurement including animal/organ positioning and potential light obstruction in the in vivo setting.

Sagittal sections of the kidneys were subsequently optically imaged (Fig. 3A), revealing a low-intensity distribution of label throughout the kidney in sections from mice dosed with unconjugated VivoTag 680 dye (Fig. 3A), whereas kidney sections from mice dosed with either GSK601A or GSK599A retained a high-intensity signal that was located almost exclusively within the renal cortex (Fig. 3A).

To confirm these observations at higher resolution, we examined kidney sections using confocal microscopy. In kidney sections from control mice dosed with VivoTag 680 dye (Fig. 3B), there was no peptide signal (Fig. 3B, magenta) (data not shown), whereas proximal tubule markers AQP1 and megalin (Fig. 3B) were colocalized in the cortex. In mice dosed with GSK599A, peptide-dye conjugate fluorescence (Fig. 3B, magenta channel) localized exclusively within segments that stained positive for AQP1 (Fig. 3B, green channel), and not within glomeruli, or distal tubules (arrows) (Fig. 3B). These observations are consistent with a mechanism, within the proximal tubules, for selectively binding and retaining the GSK601A and GSK599A peptide-dye conjugates.

Furthermore, we performed high-resolution MRI to coregister these anatomic images with our 3D optical FMT images to

address the relative distribution and semiquantitative signal localization with the kidney of the GSK599A and GSK601A peptides. Coregistration of FMT/magnetic resonance images revealed highly specific kidney localization of both GSK601A and GSK599A 1 hour after dosing (Fig. 4, A–D). The quantitative analysis of the FMT-MRI to compare the relative anatomic distribution of GSK599A and GSK601A 1 hour postinjection in cortical and noncortical regions of the kidney showed a non-significant trend of increased medullary accumulation of the smaller GSK601A peptide compared with the cortex (Fig. 4E). For GSK599A, there was a more equivalent distribution between the medullary and cortex signals (Fig. 4E). In contrast to the ex vivo images where the peptide signal was concentrated in cortex (Fig. 3), the in vivo FMT/MRI signal was more equivalent in the cortex and medulla, likely due to the filtration of dye into the medullary space in vivo and this signal being lost in the ex vivo setting.

Imaging of Renal Targeting KE Peptide in JCK Mice. After establishing the kidney localization of KE peptide-dye conjugates in control mice, we extended our study to a mouse model of polycystic kidney disease, the JCK mouse. This mouse strain displays consistent and rapid development of kidney cysts over several months and has been extensively used to evaluate therapeutic agents. In our study, 14-week-old JCK mice developed substantial and numerous cysts in the kidney (Fig. 5C). In these JCK mice, we observed a renal-specific optical signal in GSK599A- and GSK601A-dosed mice with no observable signal in

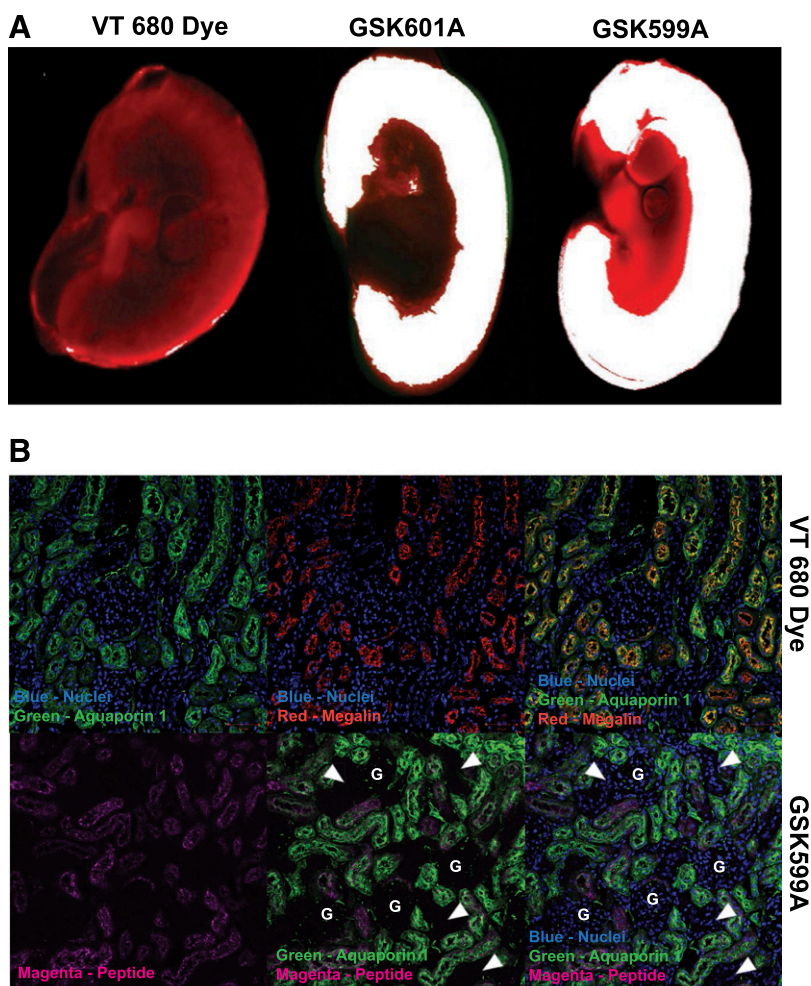


Fig. 3. High-resolution ex vivo optical imaging of kidney from mice treated with VivoTag 680 dye, GSK599A, and GSK601A and confocal immunohistochemical microscopy. (A) Representative high-resolution ex vivo optical image of VivoTag 680 dye, GSK599A, and GSK601A mouse kidneys. (B) Representative confocal images of the cortex of a kidney treated with VivoTag 680 dye (top panels) stained for proximal tubules marker AQP1 (green), megalin (red), and DAPI (blue). The bottom panels are representative confocal images of the kidney cortices of mice treated with GSK599A and stained with AQP1 (green), peptide (magenta), and DAPI (blue). Other structures including glomeruli (G) as well as distal and collecting tubules (arrows) are labeled.

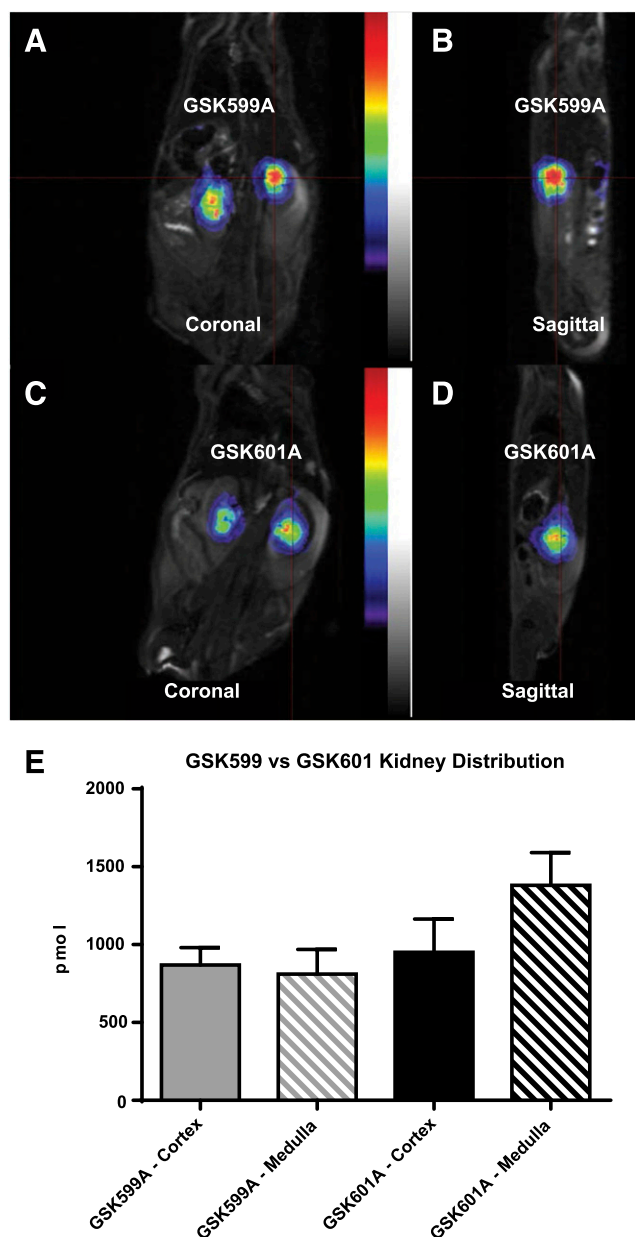


Fig. 4. Coregistration of VivoTag 680 dye signaling with FMT/MRI analysis (A and B) Coregistered MRI and FMT coronal and sagittal images of a representative control mouse 1 hour after the injection of GSK599A. (C and D) Coregistered MRI and FMT coronal and sagittal images of a representative animal 1 hour after the injection of GSK601A. (E) Quantitative analysis of cortical and medullary signals. The variations in optical signals in cortex and medulla in both treated groups are not statistically significant ($P > 0.05$), (nonparametric, paired t test). $n = 3-6$; error bars indicate mean \pm S.E.M.

the VivoTag 680 dye-treated mice (Fig. 5, A and B). High-resolution ex vivo images in VivoTag 680 dye-treated mice showed generalized, nonspecific distribution in the kidney, whereas in GSK599A- and GSK601A-treated mice there was a punctate, nonuniform signal specific to the renal cortex (Fig. 5B). This pattern of peptide distribution was not observed in healthy mice (Fig. 3). High-resolution confocal microscopy in a representative mouse dosed with GSK599A revealed distended tubules/cysts (Fig. 5D, cyst label) and complete overlap of AQP1 (green) and megalin (red) signal (Fig. 5D). The confocal image confirmed the localization of the peptide in the proximal tubules (Fig. 5D, magenta). Peptide-dye conjugate was localized in

niches underneath the cyst lining, and was completely colocalized with megalin and AQP1 immunoreactivity (Fig. 5D). Importantly, the renal cysts were negative for AQP1 and megalin immunoreactivity, and indicate that they did not bind and internalize peptide-dye conjugates (Fig. 5D).

Megalyn Protein Expression in Human Renal Carcinoma. To expand our understanding of how renal pathology might affect megalin expression in human disease, we evaluated megalin protein expression in several types of renal cancer tissues (Fig. 6). Review of the H&E-stained tissues confirmed the normal and neoplastic diagnoses provided by the vendor. Normal human kidney tissue demonstrated specificity of megalin expression exclusively with structures consistent with proximal tubules (Fig. 6; Table 1). Multiplex immunofluorescent studies using megalin and AQP1 IHC demonstrated that megalin expression is restricted to AQP1-positive proximal tubules of normal kidney tissue as well as neoplastic cells of ccRCC (Fig. 6). Tissue specimens from a donor with a diagnosis of RCC demonstrated that 90% of the ccRCC cases and 57% of the papillary RCC (pRCC) cases express megalin in the neoplastic cells (Fig. 6; Table 1). We did not detect megalin expression in any samples we evaluated from chromophobe RCC (chRCC) tissue (Fig. 6A). Rabbit IgG isotype IHC controls did not exhibit specific staining (Fig. 6A, right panels). We performed a more detailed analysis with normal kidney and ccRCC samples (Fig. 6B). Significant overlapping expression pattern between AQP1 and megalin was observed in both normal kidney sections and ccRCC tumors (Fig. 6B). It is worth noting that the overall number of tumor cases we reviewed is small and analysis of additional tumor samples are needed to draw broader conclusions.

Discussion

The tissue-specific delivery of therapeutic agents has been the focus of intensive investigations to enhance efficacy and minimize toxicity. Exploratory modalities have been evaluated to selectively target molecules in tissues such as the heart (Kanki et al., 2011; Zahid et al., 2018), tumors (Liu et al., 2017), and the liver (Mishra et al., 2013). Recently, studies have attempted to identify and characterize mechanisms that could selectively target therapeutic agents to the kidney, a concept that could expand the limited number of treatment options for chronic kidney disease by increasing the tolerability and/or limiting the extrarenal toxicity of experimental therapeutics. Peptides with short KE (KKEEE)_nK repeats, have been reported to efficaciously target small molecules to proximal tubule cells within the renal cortex of rats and multiple strains of mice (Wischnjow et al., 2016). In the current study, we extended these results and investigated whether these (KKEEE)_nK peptides could selectively target the NIR dye VivoTag 680 to the kidney, whether this targeting was consistent with megalin-dependent internalization by proximal tubule epithelial cells, and how this distribution would be altered in kidneys from mice with polycystic kidney disease phenotype.

We decided to perform optical imaging for these studies since the method does not require the use of radioactive labels unlike positron emission tomography. Using this methodology, we demonstrated that the VivoTag 680 dye signal heterogeneously distributes to the kidneys of healthy mice shortly after intravenous dosing (Fig. 2), after which it is not detectable above the baseline optical signal at 1 hour postdose. Postmortem optical imaging revealed low-intensity

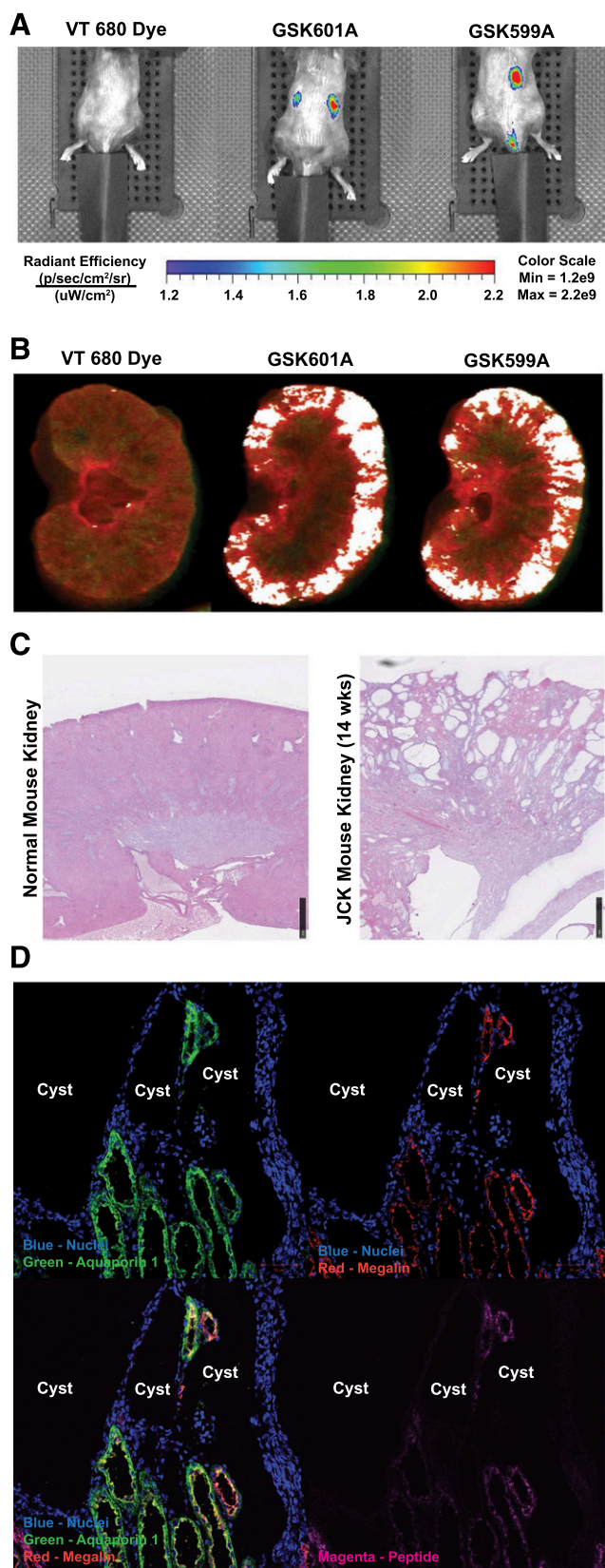


Fig. 5. In vivo and ex vivo optical imaging in JCK mouse. (A) In vivo images of 14-week-old JCK mice showing the accumulation of GSK599A and GSK601A in the kidney at 1 hour postdose. Only one kidney was observable in the GSK599A group due to positioning of the mouse in the optical scanner. (B) Ex vivo images of 14-week-old JCK kidneys (white is a saturated signal). (C) H&E-stained images of kidney sections from normal

dye signals above background signals in all harvested organs (Fig. 2), particularly liver and kidney, organs that receive a large fraction of cardiac output and play roles in the clearance of xenobiotics. In marked contrast, both KKEEE-based peptide-dye conjugates, GSK599A and GSK601A, were detected almost exclusively within the kidney, consistent with selective renal targeting and retention of the KKEEE-based peptide conjugates. Although determining the molecular receptor for these renal-targeting peptides was beyond the scope of the present investigation, multiple lines of evidence support the hypothesis that megalin plays a key role in the uptake of these peptide conjugates. Within the kidney, megalin is located on the apical surface of proximal tubule epithelial cells where it binds and internalizes filtered peptides and low molecular weight proteins. Indeed, both mice (Lehste et al., 1999) and humans (Storm et al., 2013) with mutations in the LRP2 gene that encodes megalin exhibit low molecular weight proteinuria. Thus, binding and reabsorption from the ultrafiltrate of targeting peptides such as the ones we employed in the current study are consistent with the well-established physiologic function of megalin.

In our experiments, both the 11-aa (GSK601A) and 16-aa (GSK599A) peptide conjugates selectively targeted the dye to the kidney cortex, whereas the 11-aa dye conjugate (GSK601A) had slightly more liver distribution, suggesting that a longer sequence with charged amino acid residues could potentially be more precise in renal targeting. Janzer et al. (2016) performed structure-activity relationship analysis to determine the effects of peptide length, charge, and sequence on kidney targeting efficiency. Additional structure-activity relationship work may be required to optimize targeting efficiency while enhancing desirable pharmacokinetic properties in specific kidney disease models.

JCK mice have robust renal cyst formation due to a mutation in ciliary kinase NEK8 (Liu et al., 2002). Although the underlying genetic mutation is distinct from human ADPKD (PKD1 and PKD2 mutations), the mutation alters the expression and distribution of the mouse orthologs of these polycystin genes (Sohara et al., 2008), resulting in consistent and relatively rapid cyst formation/expansion and decline in renal function (Smith et al., 2006). In polycystic JCK mice, GSK599 similarly accumulated in the renal cortex compared with healthy SKH1 control mice, and largely overlapped with megalin- and AQP1-positive cells. In comparison with normal mice kidneys, the distribution of KKEEE-conjugated dye within the cortex of JCK mice was limited and followed an irregular pattern (Fig. 5). Interestingly, the dye localized to cells directly underneath the cyst lining epithelium, rather than the cyst lining itself. Confocal imaging revealed almost no staining for the proximal tubule marker AQP1 or megalin within the cortical cells lining the most distended and largest cysts, whereas the less distended regions retained expression of both AQP1 and megalin (Fig. 5, green and red, respectively). We observed peptide-dye conjugate fluorescence only within these latter regions, demonstrating that the cyst-lining cells that have potentially ceased expressing AQP1 and megalin have also lost their

and 14-week-old JCK mice. Black scale bar, 1 mm. (D) Four confocal microscopy images of cyst areas with AQP1 (green), DAPI (blue), megalin (red), and GSK599A (magenta) staining in 14-week-old JCK mouse kidney dosed with GSK599A. Max, maximum; Min, minimum.

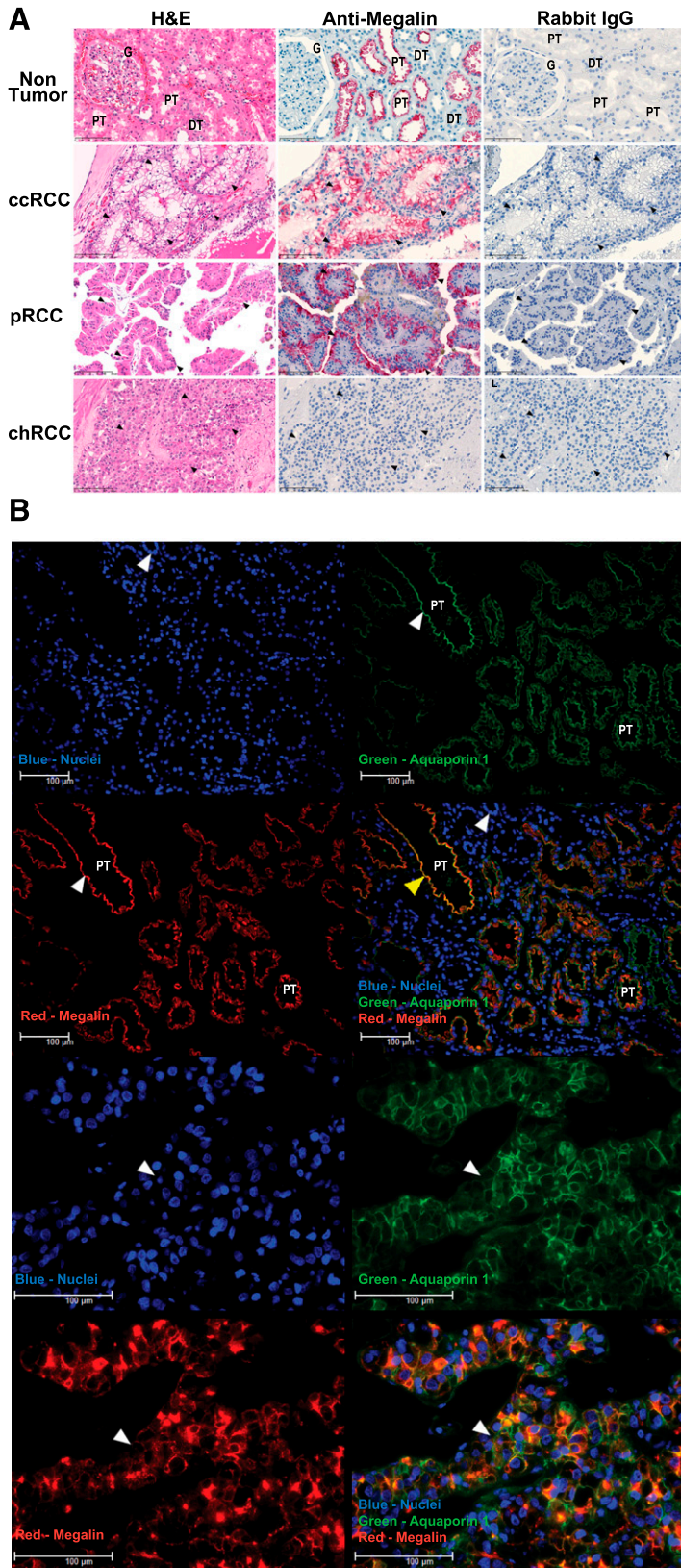


Fig. 6. Megalin expression in normal human kidney and renal tumors. (A) Megalin expression in normal kidney and tumors, including ccRCC, pRCC, and chRCC. Scale bar, 100 μ m. H&E-stained TMA cores (left panels) are included to demonstrate expected normal or neoplastic morphology. Middle panels are IHC-stained cores for megalin; cells expressing megalin are red with blue nuclei. Right panels are matched isotype-negative control sections and are absent of any nonspecific staining, showing only the blue nuclear counterstain. DT, distal tubule; G, glomerulus; PT, proximal tubule. Arrowheads demonstrate areas of neoplastic cells. (B) Normal kidney (top panels) and ccRCC kidney (bottom panels) sections stained for megalin (red) and DAPI (blue). Scale bar, 100 μ m.

Normal human kidney

Clear Cell Renal Carcinoma (ccRCC)

ability to bind and/or retain peptide-dye conjugates. Consistent with our findings, the loss of megalin expression in mature cysts was also reported in *pkd1* knockout mice (Ahrabi et al., 2010). In addition, a rat model of ADPKD showed that

the loss of endocytosis capacity was likely associated with reduced megalin expression (Obermuller et al., 2001). In humans, there has been debate as to the specific cellular origin of cysts. Studies by Grantham et al. (1987), involving

the lineage of human cyst cells, suggested that cyst epithelium is derived from proximal tubules as well as from the collecting duct, glomerular visceral tissues, and other undetermined, nontypical tubule origin.

Although our data suggest the KE peptide does not directly localize to the cyst lining, targeting megalin-positive proximal tubular cells with this approach may still be appropriate for ADPKD due to the proximity of the megalin-positive cells to the cyst lining itself and underlying stromal tissues. Depending upon the properties of the molecule, the extent of target engagement needed for efficacy, and the renal microenvironment, this targeted approach could enable the enrichment of therapeutic agents specifically in affected cells or niches within the kidney and minimize unwanted effects on other unaffected tissue or organs. Our data validate the kidney cortex-specific distribution of these peptide-dye conjugates and lay the foundation for additional investigative work into other kidney diseases, particularly those involving the proximal tubules such as renal tubular acidosis, Dent's disease, and amino acid transport diseases (Nakhoul and Batuman, 2011).

RCC is a group of malignancies arising from the epithelium of the renal tubules and represents over 90% of renal malignancies (Ebler et al., 2004). Included in this group are ccRCC, pRCC, and chRCC, with ccRCC accounting for about 70% of the cases reviewed (Jennette et al., 2015). It has been demonstrated ultrastructurally that ccRCC arises from epithelial cells of the renal convoluted tubule and that AQP1 expression in ccRCC and pRCC is significantly greater than in chRCC, oncocytomas, and collecting duct tumors (Oberling et al., 1960; Maunsbach et al., 1997; Huang et al., 2009). Our study represents the first IHC report of megalin expression in human ccRCC and pRCC. Our results, albeit with a small collection of RCC cases, indicate that a significant portion of ccRCC and pRCC cases are megalin positive and warrant additional studies. The targeted delivery strategy described here could potentially be applicable to RCC tumor treatment.

The dependency of this peptide-based delivery mechanism on the presence of megalin prompts some intriguing questions regarding the optimal design of targeting agents and the most suitable disease indications. Megalin mediates reuptake of glomerular filtrated protein and small peptides to maintain protein homeostasis. Disruption of this gene is associated with low molecular weight proteinuria and progression to end-stage renal disease (Eshbach and Weisz, 2017). This mechanism dictates that the putative kidney-targeting agent will likely be a small molecule rather than larger proteins such as antibodies conjugated to the targeting peptide that is resistant to proteolytic environments in circulation and in filtered urine, and that it be taken up via endocytosis into targeted megalin-positive proximal tubular cells. The drug will then be decoupled or released from the conjugate and migrate to its true target site for therapeutic action inside the cell. In this regard, targeting the therapeutic small molecule to the kidney is merely the first step. The accumulation of drug in the proper cell types in sufficient concentrations, the enabling of the release of the therapeutic moiety, and the achievement of biologic efficacy would all constitute additional challenges for a successful targeted, kidney-specific delivery. Additionally, whether this megalin-based targeting approach will be effective in patients with existing proteinuria, where filtered proteins may compete with targeting vectors for megalin binding, such

as those in later stages of chronic kidney disease or diabetic kidney disease, is another uncertainty that warrants further investigation.

In summary, our results represent the first imaging study of a peptide-based renal-targeting approach in a mouse model of human ADPKD. Highly enriched renal-specific targeting was achieved, and peptide-dye conjugates were localized in megalin-positive renal proximal tubular cells underneath the cyst lining. As such, this may represent an attractive strategy to target therapeutic agents to treat ADPKD and other tubular renal diseases. Additionally, megalin-positive ccRCC may also be a suitable disease for this modality.

Acknowledgments

We thank Robert Willette and Luke Devey of GlaxoSmithKline plc for their support of this project.

Authorship Contributions

Participated in research design: Lenhard, McAlexander, Virtue, Lee, Jucker, and Hu.

Conducted experiments: Lenhard, Fieles, Skedzielewski, Rambo, Trinh, and Geske.

Contributed new reagents or analytic tools: Lenhard, Fieles, Skedzielewski, Cheng, Isidro-Llobet, Nadin, Geske, and Klein.

Performed data analysis: Lenhard, McAlexander, Virtue, Fieles, Skedzielewski, Rambo, Trinh, Hong, Geske, Klein, and Jucker.

Wrote or contributed to the writing of the manuscript: Lenhard, McAlexander, Virtue, Jucker, and Hu.

References

- Ahrabi AK, Jouret F, Marbaix E, Delporte C, Horie S, Mulroy S, Boulter C, Sandford R, and Devuyt O (2010) Glomerular and proximal tubule cysts as early manifestations of Pkd1 deletion. *Nephrol Dial Transplant* **25**:1067–1078.
- Chapman AB, Devuyt O, Eckardt KU, Gansevoort RT, Harris T, Horie S, Kasiske BL, Odland D, Pei Y, Perrone RD, et al.; Conference Participants (2015) Autosomal-dominant polycystic kidney disease (ADPKD): executive summary from a kidney disease: improving global outcomes (KDIGO) controversies conference. *Kidney Int* **88**:17–27.
- Christensen EI and Birn H (2002) Megalin and cubilin: multifunctional endocytic receptors. *Nat Rev Mol Cell Biol* **3**:256–266.
- De S, Kuwahara S, and Saito A (2014) The endocytic receptor megalin and its associated proteins in proximal tubule epithelial cells. *Membranes (Basel)* **4**:333–355.
- Ebler JN, Sauter G, Epstein G, and Sesterhenn IA (2004) *World Health Organization Classification of Tumours. Pathology and Genetics of Tumours of the Urinary System and Male Genital Organs*, IARC Press, Lyon, France.
- Eshbach ML and Weisz OA (2017) Receptor-mediated endocytosis in the proximal tubule. *Annu Rev Physiol* **79**:425–448.
- Grantham JJ, Geiser JL, and Evan AP (1987) Cyst formation and growth in autosomal dominant polycystic kidney disease. *Kidney Int* **31**:1145–1152.
- Huang Y, Murakami T, Sano F, Kondo K, Nakaigawa N, Kishida T, Kubota Y, Nagashima Y, and Yao M (2009) Expression of aquaporin 1 in primary renal tumors: a prognostic indicator for clear-cell renal cell carcinoma. *Eur Urol* **56**:690–698.
- Janzer M, Larbig G, Kübelbeck A, Wischnjow A, Haberkorn U, and Mier W (2016) Drug conjugation affects pharmacokinetics and specificity of kidney-targeted peptide carriers. *Bioconjug Chem* **27**:2441–2449.
- Jennette JC, D'Agati VD, Olson JL, and Silva FG (2015) *Heptinstall's Pathology of the Kidney*, 7th ed, Wolters Kluwer, Philadelphia.
- Kanki S, Jaalouk DE, Lee S, Yu AY, Gannon J, and Lee RT (2011) Identification of targeting peptides for ischemic myocardium in vivo phage display. *J Mol Cell Cardiol* **50**:841–848.
- Leheste JR, Rolinski B, Vorum H, Hilpert J, Nykjaer A, Jacobsen C, Aucouturier P, Moskaug JO, Otto A, Christensen EL, et al. (1999) Megalin knockout mice as an animal model of low molecular weight proteinuria. *Am J Pathol* **155**:1361–1370.
- Liu S, Lu W, Obara T, Kuida S, Lehoczky J, Dewar K, Drummond IA, and Beier DR (2002) A defect in a novel Nek-family kinase causes cystic kidney disease in the mouse and in zebrafish. *Development* **129**:5839–5846.
- Liu X, Lin P, Perrett I, Lin J, Liao YP, Chang CH, Jiang J, Wu N, Donahue T, Wainberg Z, et al. (2017) Tumor-penetrating peptide enhances transcytosis of silicosis-based chemotherapy for pancreatic cancer. *J Clin Invest* **127**:2007–2018.
- Maunsbach AB, Marples D, Chin E, Ning G, Bondy C, Agre P, and Nielsen S (1997) Aquaporin-1 water channel expression in human kidney. *J Am Soc Nephrol* **8**:1–14.
- Mishra N, Yadav NP, Rai VK, Sinha P, Yadav KS, Jain S, and Arora S (2013) Efficient hepatic delivery of drugs: novel strategies and their significance. *BioMed Res Int* **2013**:382184.
- Müller RU and Benzing T (2018) Management of autosomal-dominant polycystic kidney disease-state-of-the-art. *Clin Kidney J* **11** (Suppl 1):i2–i13.

- Nakhoul N and Batuman V (2011) Role of proximal tubules in the pathogenesis of kidney disease. *Contrib Nephrol* **169**:37–50.
- Oberling C, Riviere M, and Haguenau F (1960) Ultrastructure of the clear cells in renal carcinomas and its importance for the demonstration of their renal origin. *Nature* **186**:402–403.
- Obermüller N, Kränzlin B, Blum WF, Gretz N, and Witzgall R (2001) An endocytosis defect as a possible cause of proteinuria in polycystic kidney disease. *Am J Physiol Renal Physiol* **280**:F244–F253.
- Smith LA, Bukanov NO, Husson H, Russo RJ, Barry TC, Taylor AL, Beier DR, and Ibraghimov-Beskrovnaya O (2006) Development of polycystic kidney disease in juvenile cystic kidney mice: insights into pathogenesis, ciliary abnormalities, and common features with human disease. *J Am Soc Nephrol* **17**:2821–2831.
- Sohara E, Luo Y, Zhang J, Manning DK, Beier DR, and Zhou J (2008) Nek8 regulates the expression and localization of polycystin-1 and polycystin-2. *J Am Soc Nephrol* **19**:469–476.
- Storm T, Tranebjærg L, Frykholm C, Birn H, Verroust PJ, Nevés T, Sundelin B, Hertz JM, Holmström G, Ericson K, et al. (2013) Renal phenotypic investigations of megalin-deficient patients: novel insights into tubular proteinuria and albumin filtration. *Nephrol Dial Transplant* **28**:585–591.
- Weimbs T, Shillingford JM, Torres J, Kruger SL, and Bourgeois BC (2018) Emerging targeted strategies for the treatment of autosomal dominant polycystic kidney disease. *Clin Kidney J* **11** (Suppl 1):i27–i38.
- Wischnjow A, Sarko D, Janzer M, Kaufman C, Beijer B, Brings S, Haberkorn U, Larbig G, Kübelbeck A, and Mier W (2016) Renal targeting: peptide-based drug delivery to proximal tubule cells. *Bioconjug Chem* **27**:1050–1057.
- Zahid M, Feldman KS, Garcia-Borrero G, Feinstein TN, Pogodzinski N, Xu X, Yurko R, Czachowski M, Wu YL, Mason NS, et al. (2018) Cardiac targeting peptide, a novel cardiac vector: studies in bio-distribution, imaging application, and mechanism of transduction. *Biomolecules* **8**:E147.

Address correspondence to: Erding Hu, GlaxoSmithKline plc (GSK), Mail Stop: UP1W-1210, 1250 South Collegeville Road, Collegeville, PA 19426. E-mail: Erding.Hu@gsk.com
